Earth and Planetary Science Letters 304 (2011) 455–467

Contents lists available at ScienceDirect

Earth and Planetary Science Letters

journal homepage: www.elsevier.com/locate/epsl

Timing and magnitude of Miocene eustasy derived from the mixed siliciclastic-carbonate stratigraphic record of the northeastern Australian margin

Cédric M. John [a,*], Garry D. Karner [b], Emily Browning [c], R. Mark Leckie [c], Zenon Mateo [d], Brooke Carson [e], Chris Lowery [c]

[a] Department of Earth Science and Engineering, Imperial College London, UK
[b] ExxonMobil Upstream Research Company, Houston, TX, USA
[c] Department of Geosciences, University of Massachusetts Amherst, USA
[d] Integrated Ocean Drilling Program, 1000 Discovery Drive, College Station, TX, USA
[e] Chevron Corporation, 1500 Louisiana, Houston, TX, USA

ARTICLE INFO

Article history:
Received 12 August 2010
Received in revised form 24 January 2011
Accepted 6 February 2011

Editor: P. DeMenocal

Keywords:
sea-level
eustasy
amplitude of sea-level change
ice volume
sequence stratigraphy
Heterozoan carbonates
Miocene
ODP Leg 194

ABSTRACT

Eustasy is a key parameter to understand sedimentary sequences on continental margins and to reconstruct continental ice volume in the Cenozoic, but timing and magnitude of global sea level changes remain controversial, especially for the Miocene Epoch. We analyzed sediment cores recovered from the Marion Plateau, offshore northeastern Australia, during Ocean Drilling Program (ODP) Leg 194 to define the mechanisms and timing of sequence formation on mixed carbonate-siliciclastic margins, and to estimate the amplitude of Miocene eustatic adjustments. We identified sequence boundaries on seismic reflection lines, significantly revised the existing biostratigraphic age models, and investigated the sedimentary response to sea-level changes across the Marion Plateau. We subdivided the Miocene sediments into three sequence sets comprising a set of prograding clinoforms, a muddy prograding carbonate ramp evolving into an aggrading platform, and a lowstand ramp evolving into a backstepping ramp. We recognized eight individual sequences dated at 18.0 Ma, 17.2 Ma, 16.5 Ma, 15.4 Ma, 14.7 Ma, 13.9 Ma, 13.0 Ma, and 11.9 Ma. We demonstrate that sequences on the Marion Plateau are controlled by glacio-eustasy since sequence boundaries are marked by increases in $\delta^{18}O$ (deep-sea Miocene isotope events Mi1b, Mbi-3, Mi2, Mi2a, Mi3a, Mi3, Mi4, and Mi5, respectively), which reflects increased ice volume primarily on Antarctica. Our backstripping estimates suggest that sea-level fell by 26–28 m at 16.5 Ma, 26–29 m at 15.4 Ma, 29–38 m at 14.7 Ma, and 53–81 m at 13.9 Ma. Combining backstripping with $\delta^{18}O$ estimates yields sea-level fall amplitudes of 27 ± 1 m at 16.5 Ma, 27 ± 1 m at 15.4 Ma, 33 ± 3 m at 14.7 Ma, and 59 ± 6 m at 13.9 Ma. We use a similar approach to estimate eustatic rises of 19 ± 1 m between 16.5 and 15.4 Ma, 23 ± 3 m between 15.4 and 14.7 Ma, and 33 ± 3 m between 14.7 and 13.9 Ma. These estimates can be combined into a eustatic curve that suggests that sea-level fell by 53–69 m between 16.5 and 13.9 Ma. This implies that at least 90% of the East Antarctic Icesheet was formed during the middle Miocene. The new independent amplitude estimates are crucial as the Miocene is the geologic Epoch for which the New Jersey margin sea-level record is poorly constrained.

1. Introduction

Eustasy (global sea-level) reflects changes in ocean volume and the amount of water in the oceans (Miller et al., 2005, Pitman and Golovchenko, 1983). It is distinct from relative sea-level that represents a combination of eustasy, sediment and water loading, and regional tectonics (fluctuation of the local datum due to subsidence or uplift, (Posamentier et al., 1988)). One of the main goals of this manuscript is to provide a new record of the timing and amplitude of eustasy for the time interval 18.0–10.4 Ma, which is still poorly constrained in other sea-level records. Constraining eustasy is crucial to the understanding of the large-scale stacking patterns that comprise the preserved stratigraphy of basins and continental margin deposits because global sea-level is one of the principal controls on sediment accommodation (i.e., the space available for sediment to be deposited within a basin). A record of the amplitude of glacio-eustatic fluctuation in the Miocene would also yield information on the large-scale dynamics of high-latitude ice sheets for that critical time interval of the Cenozoic (Bartek et al., 1991).

However, reconstructing the timing and amplitude of eustatic changes has proved a challenging task. The pioneering works of the Exxon team (Haq et al., 1987, 1988, Vail and Hardenbol, 1979), though widely cited, have been also increasingly questioned. Aside from some inconsistencies in the timing of eustatic changes, a particular problem

* Corresponding author.
E-mail address: cedric.john@imperial.ac.uk (C.M. John).

0012-821X/$ – see front matter © 2011 Elsevier B.V. All rights reserved.
doi:10.1016/j.epsl.2011.02.013

of the Haq et al. (1987, 1988) curve is that the amplitude variations are at least 2.5 times larger than suggested by other studies (John et al., 2004, Miller et al., 2005). In an effort to calibrate the Haq et al. (1987, 1988) curve, the Ocean Drilling Program (ODP) has dedicated multiple expeditions to understanding the timing and amplitude of eustatic variations (Camoin et al., 2007, Eberli et al., 1997, Isern et al., 2002, Miller et al., 1998, Mountain et al., 1994). To date, the New Jersey margin transect (ODP Legs 150, 150X, 174, 174X, and Integrated Ocean Drilling Program (IODP) Expedition 313, (Miller et al., 1998, Mountain et al., 1994, Mountain et al., 2009)) recovered the longest and most detailed stratigraphic record to help constrain eustasy. But despite its success, the New Jersey margin transect is unable to supply an unambiguous record of eustasy because of the various assumptions made in the analyses. For example, it has been assumed that the only tectonic contribution to accommodation generation across the New Jersey margin is from thermal subsidence (Kominz et al., 2008). Local tectonic contributions to accommodation cannot be ruled out and thus remains a potential source of error in the amplitude estimate for this margin (Browning et al., 2006). A second problem specific to the New Jersey margin transect is that the onshore sequences are located high on the continental shelf: sedimentation is only possible during stages of high sea-level. That is, the up dip stratigraphic record consists of a series of stacked highstand deposits dominated by unconformities. Consequently, the amplitude estimates for the Miocene are the least constrained on the New Jersey margin (Kominz et al., 2008).

Deep-sea records of oxygen isotopes offer another method to investigate the timing of glacio-eustatic adjustment for the Cenozoic (Miller et al., 1987, 1991a,b, Zachos et al., 2001). However, the isotope records alone are unable to unambiguously resolve the magnitude of eustasy due to the dual control of water temperature and ice volume on the $\delta^{18}O$ of calcite, and the scarcity of studies coupling $\delta^{18}O$ with independent temperature estimates (Billups and Schrag, 2002, Shevenell et al., 2004, 2008). Furthermore, the calibration between the rate of oxygen isotope changes in seawater and the unit of ice volume stored at high latitude is only constrained for the Pleistocene (Fairbanks and Matthews, 1978). The lack of a well defined sea-level curve, especially for the Miocene, emphasizes the need for additional stratigraphic records to augment the studies of the New Jersey margin.

2. Background and objectives

A region that holds promise for studying Miocene eustasy is the Marion Plateau carbonate system drilled offshore northeast Australia (Fig. 1) during ODP Leg 194 (Isern et al., 2002). The Marion Plateau stratigraphic record is suitable for precise sea-level reconstructions and thus to assess eustatic timing and magnitude. It provides a depth transect from a shallow carbonate platform to deeper water sites where a robust chronostratigraphic framework and an oxygen isotope record can be established. Leg 194 was designed to quantify the amplitude of the middle Miocene eustatic fall, and it partly achieved its goal by using the geometrical relationship between a highstand carbonate platform at Site 1193 and lowstand ramp deposits at Site 1194 (Isern et al., 2002). Post cruise work refined the backstripping model used for this estimate and when combined with oxygen isotope constrains, bracketed the magnitude of the long-term (13.5–11.0 Ma) sea-level fall to 50.0 ± 5.0 m (John et al., 2004). This paper attempts to extract a sub-million year eustatic signal from the Marion Plateau data, comparable to the isotopic record of Miller et al. (1991a,b).

ODP Leg 194 cored a transect of wells ("holes" in ODP terminology) from the top of the drowned Northern Marion Platform (hereafter "NMP") to the distal slope of this system (hereafter named the "NMP transect", comprising in order of increasing water-depth ODP sites 1193, 1194, 1192, and 1195, Fig. 1). The current water-depth at

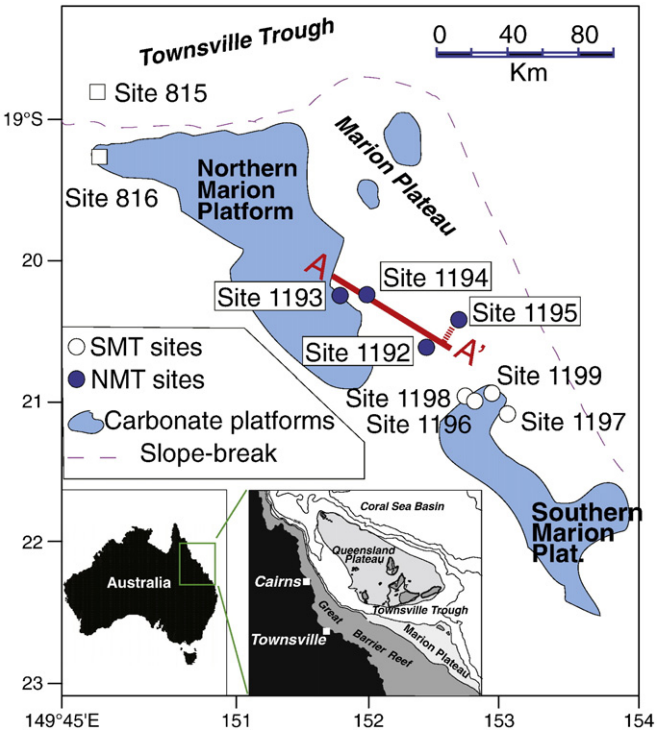

Fig. 1. Location of the study (Modified from John and Mutti, 2005).

these locations ranges from 348 m at site 1193 to 420 m at site 1195 (Table 1). Site 1193 is located on top of the NMP, where paleo water depths are estimated to range from >200 to <30 m during the Miocene (Table 1). Sites 1194, 1192 and 1195 are periplatform locations throughout the Miocene. Site 1194 is located east of the NMP, on an upper slope location, with paleo water depth varying between >200 m and <60 m during the Miocene (Table 1). Sites 1192 and 1195 are located southeastward of site 1194, in a distal periplatform location with paleodepth in excess of 150 m (Table 1). Isern et al. (Isern et al., 2002) divided the Oligocene to Holocene sediments of the Marion Plateau into four seismic Megasequences. These megasequences were defined in terms of large-scale changes in the sedimentary architecture of the plateau bounded by unconformities. Megasequence A (MSA) represents deposition of siliciclastic sediment on the plateau as it subsided below base level in the Paleocene to Oligocene, Megasequence B (MSB) represents deposition of carbonate on the plateau during the Miocene, and Megasequences C and D represent deposition of contourites and sediment drifts after the final drowning of the carbonate platform.

This paper focuses on the early to late Miocene carbonate record of Megasequence B and its implications for Miocene eustasy. Our study has three main objectives: 1) to understand the stratigraphic response of the mixed carbonate-siliciclastic sequences from the Marion Plateau to Miocene base level changes, 2) to improve the dating of the identified sequences, and 3) to reconstruct the timing and amplitude of Miocene eustasy based on Marion Plateau sequences.

To achieve our first objective we need to understand the detailed stratigraphic architecture of the Marion Plateau. Seismic stratigraphy and drilling data suggest that the NMP foundered during the middle Miocene and a lowstand ramp was established at site 1194 (Isern et al., 2002, 2004). However, the finer scale mechanism of sequence formation and the nature of sequences in the more distal part of the basin remain speculative. Understanding the sequence stratigraphic framework of the NMP transect, especially in the better dated and recovered distal slope (periplatform) sediments, is essential to extract a more highly resolved

Table 1
Age, stratigraphic interpretation, and position of the sequences defined in this study. Paleo-water depth estimates before and after each eustatic adjustment is indicated for sites 1193 and 1194 (paleo water-depth estimates are compiled from Hallock et al., 2006; Isern et al., 2002). This data is used in the backstripping calculation.

ODP Site 1193 (platform) Current water depth: 348 m	Depth of the pick and selection criteria	440.0 mbsf (908 ms), base of MSB as defined shipboard	385.1 mbsf (811 ms),	254.0 mbsf, (697 ms) base of bryozoan mound facis	169.0 mbsf, (672 ms)	85.4 mbsf, (625 ms) Major change within NMP, exposure surface	35 mbsf, (508 ms) top NMP, erosional surface and hardground.	Platform exposed during eustatic fall and drowned during subsequent eustatic rise: hiatus		
	Paleowater depth before eustatic adjustment	<60 m	<30 m	> 100 m	30-100 m	<30 m	<30 m			
	Paleowater depth after eustatic adjustment	<60 m	<0 m (exposed)	Truncation visible in seismic: current erosion?	< 0 m (exposed)	<0 m (exposed)	<0 m (exposed)			
ODP Site 1194 (Upper Slope) Current water depth: 374 m	Depth of the pick and selection criteria	421.1 mbsf (893 ms), base of MSB as defined shipboard	385 mbsf (860 ms)	243.0 mbsf, (765 ms),	206.0 mbsf (746 ms),	170.0 mbsf (690 ms),	160.0 mbsf (672 ms),	123.35 mls (645 ms),	Eroded, corresponds to base of MSD and a hardgroud at 114.7 mbsf	
	Paleowater depth before eustatic adjustment	? (basalt)	< 100 m	> 100 m	> 100 m	> 100 m	> 100 m	30-50 m		
	Paleowater depth after eustatic adjustment	<100 m	< 0 m (exposed)	20-30 m	> 100 m	< 60 m	30-50 m	30-50 m		
ODP Site 1192 (Distal Slope) Current water depth: 375 m	Depth of the pick and selection criteria	Not cored (985 ms)	Not cored (945 ms)	Not cored (908 ms)	325.9 mbsf, (871 ms)	310.7 mbsf, (851 ms) base GI-2	288.6 mbsf, (832 ms) i	Not recovered, projected at 282 mbsf based on age model (827 ms)	262.4 mbsf (811 ms),	236.7 mbsf (773 ms),
ODP Site 1195 (Distal Slope) Current water depth: 420 m	Depth of the pick and selection criteria	435 mbsf (1006 ms)	403.0 mbsf (979 ms),	367.0 mbsf, (947 ms),	321.5 mbsf (918 ms),	285.9 mbsf (881 ms),	263.2 mbsf (859 ms),	256.6 mbsf (852 ms),	249.0 mbsf (840 ms),	230.0 mbsf (812 ms),
Corresponding glauconitic layer		None	None	GI-1	GI-2	GI-3	GI-4	GI-5	GI-6	None
Isotope stratigraphy		MBi-2†	MBi-3†	Uncertain: Mi2/MLi-1?	Mi2a	Mi3a/MSi-1	Mi3b	Mi4 /MSi-3†	MSi-4? Mi5?	Unkown
Ages used in this study (see Supplementary Table S3)		18.0 Ma	17.2 Ma	16.5 Ma	15.4 Ma	14.8 Ma	13.9 Ma	13.0 Ma	12.1 Ma	10.9 Ma
Sequence stratigraphy	**Sequence**	MSB1.1	MSB1.2	MSB2.1	MSB 2.2	MSB 2.3	MSB 3.1	MSB 3.2	MSB 3.3	MSC1.1
	Sequence set	MSB1		MSB2			MSB3			MSC

** Ages from Miller et al., 1998
* Orbitally tuned ages from Westerhold et al., 2005
# Orbitally tuned ages from Holbourn et al., 2005
† Ages from Abreu and Anderson, 1998

record of sea-level variation than defined by previous works (Isern et al., 2002). In addition, this sequence stratigraphic framework will provide insight into the stratigraphic response of mixed carbonate-siliciclastic sedimentary systems to sea-level changes, a theme recently highlighted as a main objective of eustatic research (Fulthorpe et al., 2008).

To achieve our second objective we need to improve the biostratigraphic constraints on the Marion Plateau, especially for the distal periplatform sites where high-resolution dating is possible. The timing of the long-term middle Miocene eustatic fall reported for the Marion Plateau is currently poorly constrained based on shipboard biostratigraphy. Isern et al. (2002) postulated that the sea-level fall recorded by ODP Leg 194 corresponds to planktic foraminifer Zones N12–N14 (12.5–11.4 Ma), but the few age constrains for the lowstand ramp site suggests that the onset of the eustatic fall was closer to 13.6 Ma (Isern et al., 2002). In our earlier work (John et al., 2004), we assumed that the Marion Plateau sequences were recording a 13.8–12.0 Ma sea-level fall corresponding to the two largest middle Miocene isotopic events Mi3 and Mi4. It is not clear that this timing is correct.

The final objective of our study is to demonstrate a link between the sequence stratigraphy of the Marion Plateau and eustatic variations, and to quantify eustatic changes. Although it has been postulated that the Marion Plateau was a passive margin and thus recorded eustatic changes (Isern et al., 2002), a clear link between eustatic forcing and Marion Plateau sedimentary sequences has never been positively established. This demonstration is a critical step towards establishing the Marion Plateau as a faithful recorder of eustatic variations.

3. Methods

Detailed methods can be found in the online supplementary material. Smear slides for nannofossil analysis were prepared using

the method of Watkins and Bergen (2003) and majority of the datum levels and their assigned ages are based on Raffi et al. (2006). Additional information on the relative position of several nannofossil species are derived from deKaenel and Villa (1996). For datum levels, we used the first occurrence ("FO"), last occurrence ("LO"), and highest common occurrence ("HCO", sensu Raffi et al., 2006) of index species. Planktic foraminiferal age datums are from the 2004 ICS Geologic timescale (Gradstein et al., 2005).

Key stratigraphic horizons were identified by comparing seismic data with core data in an iterative fashion. The seismic dataset is a PDF version of high-resolution multichannel seismic profiles acquired in 1999 by the Australian Geological Survey Organization [AGSO], and to which standard multi- channel processing suite had been applied (Isern et al., 2002, 2004). Sequence boundaries were identified based both on truncation of seismic reflectors (i.e., erosional surfaces) on seismic lines and on evidence of sediment condensation and isotope stratigraphy in the cores. The core to seismic integration was achieved using the relationship between depth in meters below seafloor (mbsf) to two-way-travel time (TWT) established by offset VSP (Vertical Seismic Profile) during ODP Leg 194 (Isern et al., 2002).

Point counting of the coarse fraction (>63 μm) of sieved sediments at sites 1192, 1194, and 1195 was done using a binocular microscope and analog point counter. Point counting characterization for the platform facies at site 1193 and the lithified "ramp" facies from site 1194 was based on shipboard thin sections (Isern et al., 2002) using a petrographic microscope. A total of 300 fragments were counted for each sample.

Sample preparation for stable isotopes followed Nathan and Leckie (2009). Stable isotope analysis on specimens of the benthic foraminifer genus *Cibicidoides* spp. were performed at the University of South Florida, College of Marine Science using a Finnigan-MAT Delta Plus XL mass spectrometer with a Kiel III automated carbonate device having an analytical precision of ± 0.08‰ for $\delta^{18}O$ and ± 0.04‰ for $\delta^{13}C$. Sr-isotope composition was measured for 3 bulk samples coming from Hole 1194B on a Finnigan MAT 262 RPQ+ in static mode at the University of Kiel (Germany). The internal precision was better than 10 ppm (2 SE), and a mean $^{87}Sr/^{86}Sr$ value of 0.710236 ± 34 (2 standard deviation) for the NIST 987 standard solution was calculated. Conservatively, we assigned an error estimate of ± 1.0 Ma to our Sr ages.

4. Results

4.1. Revised age models and stratigraphic correlations

We identified 15 calcareous nannofossil events and 6 additional planktic foraminifer events (Table S1), and combined the new biostratigraphic constraints with shipboard datums to obtain 11 lines of correlation (LOC). We trace the LOCs from the upper to lower slope (sites 1194, 1192, 1195, and Fig. 2). Age models for sites 1194, 1192, and 1195 are reconstructed using the new age data points (Table 1, and Fig. 3). The stratigraphic position of many of the revised datum levels differs significantly from the shipboard age models (Isern et al., 2002), in part because our sampling resolution (typically 0.5 m to 1.5 m) is much higher than shipboard (9.8 m). The best age constraints were obtained at Hole 1195B (Fig. 3), where our high-resolution revised age model agrees well with shipboard magnetostratigraphy (Isern et al., 2002) and published stable isotope markers (John and Mutti, 2005), thus reconciling the different observations. For the interval around 260 mbsf at Site 1195 the revised ages are up to 1.8 myr older than shipboard data (Fig. 3). Strontium isotope results for the three samples of Hole 1194B yielded results between 0.7088 and 0.7086. The values were converted into age using the published calibration curve (Oslick et al., 1994). Ages obtained by these conversions are 15.6 ± 0.7 Ma, 16.6 ± 0.7 Ma and 17.4 ± 0.7 Ma, respectively (Fig. 3). The improved age model and correlations of the Marion Plateau sequences offer a robust record for constraining the timing of eustatic variations across the plateau.

4.2. Seismic stratigraphy of Megasequence B ("MSB")

We propose a subdivision of MSB into a nested hierarchy of sequences comprising (from larger to smaller unit) sequence sets, individual sequences, parasequence sets, and individual parasequences (the smallest unit). A sequence set represents a distinct mode of sedimentation within Megasequence B, e.g., prograding clinoforms or aggrading platforms. Sequence sets are typically tens of meters thick on the Marion Plateau, and are composed of individual sequences. Individual sequences are bounded by erosional unconformities (sequence boundaries). Sequence boundaries are named after the sequence immediately above them, e.g., sequence boundary MSB1.1 marks the base of sequence MSB1.1, which itself marks the base of sequence set MSB1.

Based on seismic geometries, we identified three sequence sets and eight sequences within MSB (Fig. 4, the position in millisecond (ms) and mbsf of each of the sequences and sequence sets are given in Table 1):

Sequence set MSB1 — Prograding slope clinoforms (~18.0 Ma–16.5 Ma): sequence set MSB1 comprises prograding carbonate clinoforms overlying the siliciclastic sequences of MSA. The upper boundary of sequence set MSB1 is marked by truncation of the up-dip portion of reflectors best seen at and immediately east of site 1193. We also observed truncation of reflectors within sequence set MSB1 west of site 1194 and east of site 1192, and recognize this as a sequence boundary dividing the sequence set into two sequences (MSB1.1, ~18.0 Ma–17.4 Ma, and MSB1.2, ~17.4–16.5 Ma, Fig. 4). The ages of sequence boundaries within sequence set MSB1 are poorly constrained (Table S3), but the interpolated ages obtained from sites 1192 and 1195 agree well with published ages for sequences MBi-2 and MBi-3 (Abreu and Anderson, 1998, Miller et al., 1998).

Sequence set MSB2 — Aggrading to prograding carbonate ramp ("MCR") to Northern Marion Platform (~16.5 Ma–13.9 Ma) the base of sequence set MSB2 is marked by the truncation of the prograding clinoforms of MSB1, visible between sites 1193 and 1194. This sequence set represents the establishment of a carbonate ramp at site 1193, first characterized by high clay content, and its subsequent development into the well cemented NMP. Sequence set MSB2 can be divided into three individual sequences based on an interpreted sequence boundary marked by limited truncation of reflectors. Sequence MSB2.1 (16.6 Ma–15.4 Ma, Table 2) shows evidences of offlapping reflectors suggesting large-scale retrogradation of the platform. A structure with mound geometry and a landward depression is faintly delineated at the proximal end of the wedge (Fig. 4). Sequence MSB2.2 (15.4–14.7, Table S3) is prograding at the base as evidenced by the migration of the shelf crest eastward from site 1193, and aggrading to retrograding at the top (Fig. 4). The lithified facies of the NMP was established within sequence MSB2.2. A biostratigraphic marker 10 meters below the first bryozoan facies at site 1193 (last occurrence of *Globigerina connecta*, 16.40 Ma, Isern et al., 2002) supports this interpretation. Our age model for site 1193 is based on chemostratigraphic correlations based on carbon and oxygen isotopes (Mutti et al., 2006), the latest biostratigraphic age constraints available for the platform (Hallock et al., 2006), and seismic stratigraphic constraints (Isern et al., 2002). The age model is also compatible with the strontium isotopes ages >15 Ma published by Ehrenberg et al. (Ehrenberg et al., 2006), but not with the Sr ages within the platform facies, which suggest that the NMP was growing until at least 10.0–9.7 Ma. One problem in applying Sr stratigraphy on the NMP is that the middle Miocene is the interval of the Cenozoic with the lowest rate of strontium isotope change per unit of time,

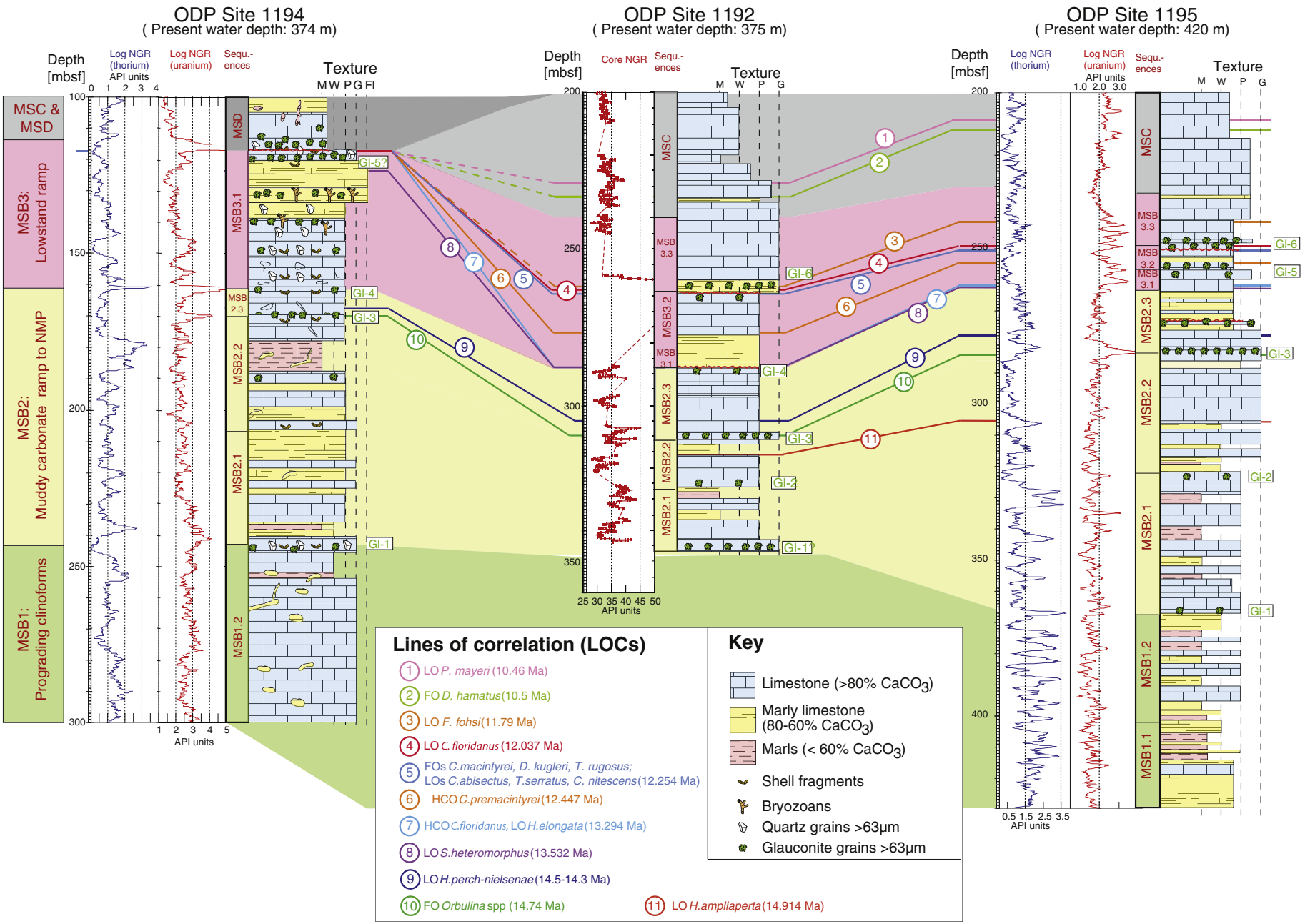

Fig. 2. Summary of the lithostratigraphy and biostratigraphic correlations for slope sites 1194, 1192 and 1195. Lines with numbers represent lines of correlation (LOC) and can be referred to Supplementary Table 1. Sequences are defined in the text and in Fig. 6. Downhole log and core natural gamma ray are from (Isern et al., 2002).

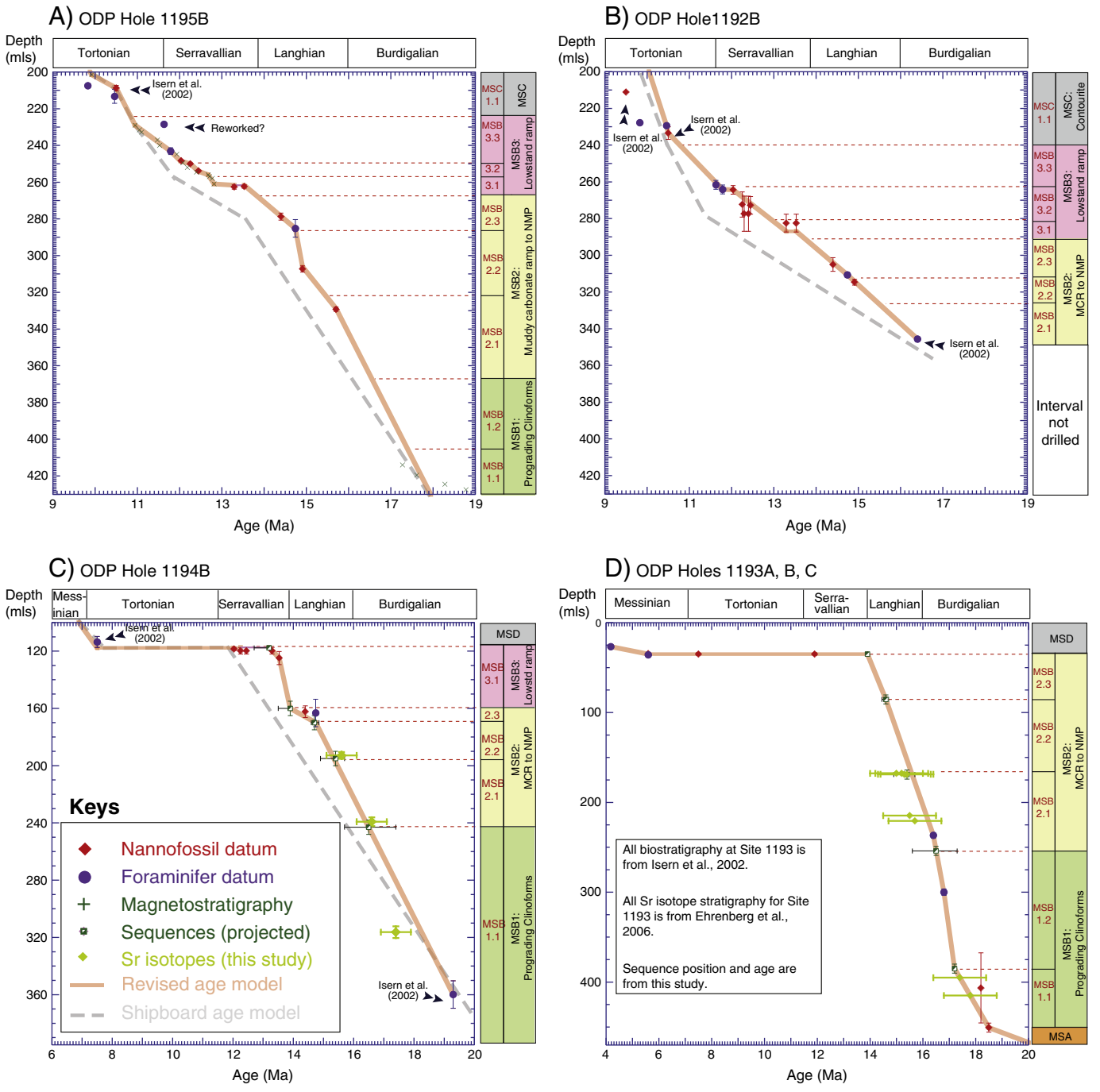

Fig. 3. Revised age model for ODP Hole 1195B. Biostratigraphic markers are from this study, unless marked with an asterisk (Isern et al., 2002). Magnetostratigraphic data are from ODP Leg 194 (Isern et al., 2002). The dashed gray lines represent the shipboard age models, the solid orange lines represent our revised age model. Shipboard magnetostratigraphy from Site 1195 agrees well with the revised age model. Sequences defined in this study are reported on the right of the graph. At Site 1194, the biostratigraphic age model is supplemented with the age and stratigraphic position of sequence boundaries identified and dated at sites 1192 and 1195, and correlated to site 1194 by tracing seismic reflectors. Dashed red lines trace the base of individual sequences. The depth of biostratigraphic markers is reported in meters logging scale (mls), which was obtained by calculating the possible range in depth of each event, taking into account core recovery and uncertainties in the position in the well of incomplete cores. This allows a tie-in with the logs and more realistic sedimentation rates to be estimated.

implying larger errors in dating (Mcarthur and Howarth, 2004). Oslick et al. (1994) have demonstrated statistically that the error in age assignment for samples younger than 15 Ma is larger than ± 1.0 m.y. If even trace amounts of dolomite or fluid inclusions with very different Sr isotope composition were unknowingly measured in the analysis of Ehrenberg et al. (Ehrenberg et al., 2006), the results would be biased towards younger apparent ages. We suspect that this is the case here. The last sequence of sequence set MSB2 is represented by the final stage of aggradation on the NMP before its final demise at 13.9 Ma. The sequence boundary for MSB 2.3 (14.7–13.9 Ma, Table S3) is recognized by a switch from mostly dolomitized platform facies to non-dolomitized facies, by marked changes in water depth following reflooding of the exposed surface, and by the presence of silt-infilled vugs and erosional surfaces.

Sequence set MSB3 — Lowstand ramp (13.9 Ma–10.9 Ma): the base of sequence set MSB3 was recognized during Leg 194 at site 1194 and correlated to the top of the NMP at site 1193 (Isern et al., 2002). Sequence set MSB3 at site 1194 is marked by truncation of the

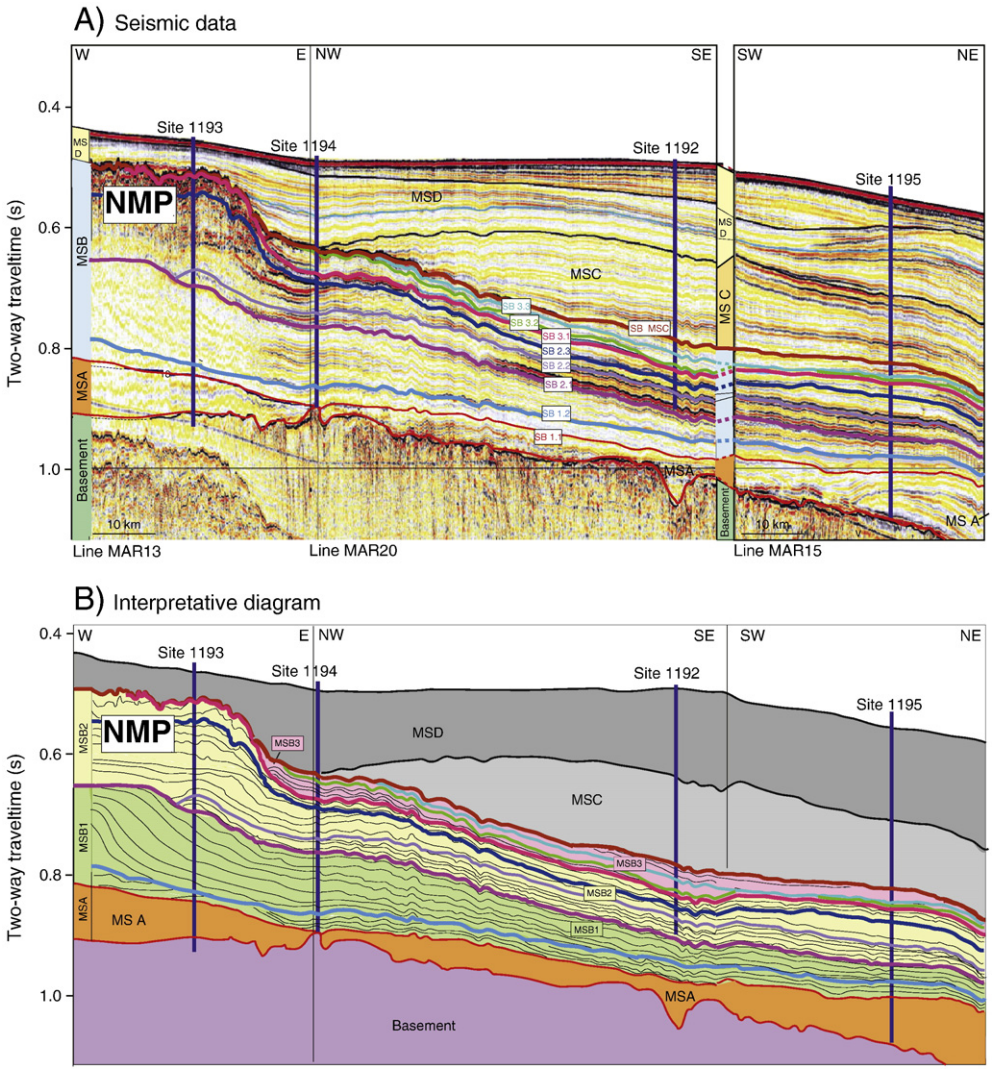

Fig. 4. A) Interpreted seismic line from (Isern et al., 2002). The seismic pick representing sequence boundaries are marked as on overlay. B) Interpretative diagram showing the seismic geometries of each sequence set within Megasequence B (MSB).

underlying clinoforms at the top of sequence set MSB3, and can be correlated basinward to sites 1192 and 1195. We divided sequence set MSB3 into three individual sequences (MSB3.1–MSB3.3) that are recognized in the cores based on evidence of condensation and increases in $\delta^{18}O$ (see discussion for details). Sequence boundary MSB3.1 corresponds to an unconformity dated at >13.5 Ma (Table S3 and Fig. 3), and is associated with isotopic event Mi3 which has an orbitally tuned age of 13.9 Ma (Holbourn et al., 2007). Reflectors in sequence set MSB3 show evidence of progradation at the base of the sequence set, and offlapping towards the top of the sequence. This geometry suggests initial lowstand conditions (prograde of a lowstand wedge), followed by rapid sea-level rise with sediments unable to "catch up" with the rise. As in sequence MSB2.1, a structure with mound geometry and a landward depression is faintly delineated at the proximal end of the wedge (Fig. 4). The upper boundary of sequence set MSB3 is characterized by truncation of the underlying

Table 2
Comparison between the ages of sequences recognized on the Marion plateau, Queensland plateau, Great Bahama bank, New Jersey margin and Haq et al. curve (Haq et al., 1987, 1988).

Marion plateau		Queensland plateau		Great Bahamas bank		New Jersey margin		EPR curve		Isotope stratigraphy
Sequence	Age (Ma)	Sequence	Age (Ma)	Sequence	Age (Ma)	Sequence	Age (Ma)	Sequence	Age (Ma)	
MSC1.1	10.9	QU5	10.3-11	I	10.7	NR	10.4	TB 3.1	11.0	N/A
MSB3.3	12.1	QU4	12.4	K	12.2	m1	11.9	TB 2.6	11.9	Mi5
MSB3.2	13.2	QU3	12.6	L	12.7	Kw-Ch	13.1			Mi4
MSB3.1	13.9					Kw3	13.8	TB 2.5	13.9	Mi3
MSB2.3	14.7					m4	14.3			Mi3a
MSB2.2	15.4			M	15.1	Kw2c	14.9	TB 2.4	15.1	Mi2a
MSB2.1	16.5	QU2	16-16.7	N	15.9	Kw2b	16.1-16.3	TB 2.3	16.5	Mi2
MSB1.2	17.2									Mbi-3
MSB1.1	18.0	QU1	18.0	O	18.3	Kw2a	18.1-18.5	TB 2.2	17.5	Mi1b/Mbi-2

reflectors marking the onset of strong bottom current and the base of Megasequence C. MSB3.2 and MSB3.3 are absent at site 1194 and immediately east of this location, suggesting erosion or non-deposition due to currents (Fig. 4).

4.3. Major temporal trends in sedimentation

We observe similarities between the % planktic foraminifer (relative to the total planktic plus benthic foraminifer population, % PF) trends at sites 1194, 1192 and 1195 (Fig. 5). The long-term trends in % PF (smooth curve, Fig. 5) at site 1195 decreased from 17 to 14.7 Ma, remained relatively constant between 14.7 and 13.9 Ma, increased stepwise at 13.9 Ma (corresponding to sequence MSB3.1), and increased within sequence set MSB3 and Megasequence C.

We recognize several glauconitic layers on the basis of our point counting (Fig. 6A). Sequence boundaries identified in sequence sets MSB2 and MSB3 correspond to glauconite-rich intervals observed within cores of the periplatform. Sequence boundary MSB 2.1 is associated with glauconitic layers (named Gl-1) at sites 1194 and 1195. Glauconite layer Gl-1 can also be seen at the base of the recovered section from site 1192, although it appears to be stratigraphically above the position of Gl-1 at other sites. A relatively weak glauconite layer at the base of MSB2.2 (15.4 Ma) referred to as Gl-2 is best seen in ODP Hole 1192B and is present at site 1195 (Fig. 6A), although glauconite abundance is low at this latter location. The base of sequences MSB2.3 and MSB3.1 are characterized by glauconite layers Gl-3 and Gl-4, respectively. Sequence boundary MSB3.2 is characterized by an erosional truncation visible in the biostratigraphic data (Fig. 2, LOC 6) and by glauconite layer Gl-5. Finally sequence boundary MSB3.3 is marked by glauconite layer Gl-6.

Platform-derived neritic fragments in the coarse fraction of the distal sites 1192 and 1195 are abundant in sequence set MSB1, decreases within sequence MSB2.1, but increases again at the base of sequence MSB2.2 (Fig. 6D). The content of platform-derived material drops sharply at the MSB2.3 sequence boundary (corresponding to oxygen event Mi3a; Miller et al., 1998), increases towards the end of this sequence, and drops abruptly again at the base of sequence MSB3.1 (corresponding to oxygen isotope Mi3). Platform derived fragments are low and decreasing in the remainder of sequence set MSB3, with the exception of one sharp peak within sequence MSB3.3 at Site 1192. At ODP Site 1195, the base of Megasequence C corresponds to low % Planktic foraminifers, higher platform derived fragments, and a slight increase in the background glauconite level.

5. Discussion

5.1. Nature of sequence boundaries and correlative surfaces

Each of the sequence boundaries observed in the seismic data corresponds within sequence set MSB2 and MSB3 to intervals rich in glauconite in the cores of the periplatform (sites 1194, 1192 and 1195). The basal surface of the glauconitic layers is characterized by an abrupt change in lithofacies and sometimes an irregular and bioturbated surface reminiscent of a firm ground. The glauconitic layers are often composed of coarser sediments and may contain fish teeth, suggesting that the glauconite and associated sequence boundaries correspond to episodes of low sedimentation on the periplatform (i.e., sediment condensation, Fig. 6). Biostratigraphic data confirm that at least sequence boundaries MSB3.1 and MSB3.3 (glauconite layers Gl 3 and Gl 6) correspond to dramatic reductions in sediment accumulation at sites 1192 and 1195 (Fig. 3). Evidence for sediment condensation during sea-level lowstands is at the core of the "highstand shedding" theory (Schlager et al., 1994) initially

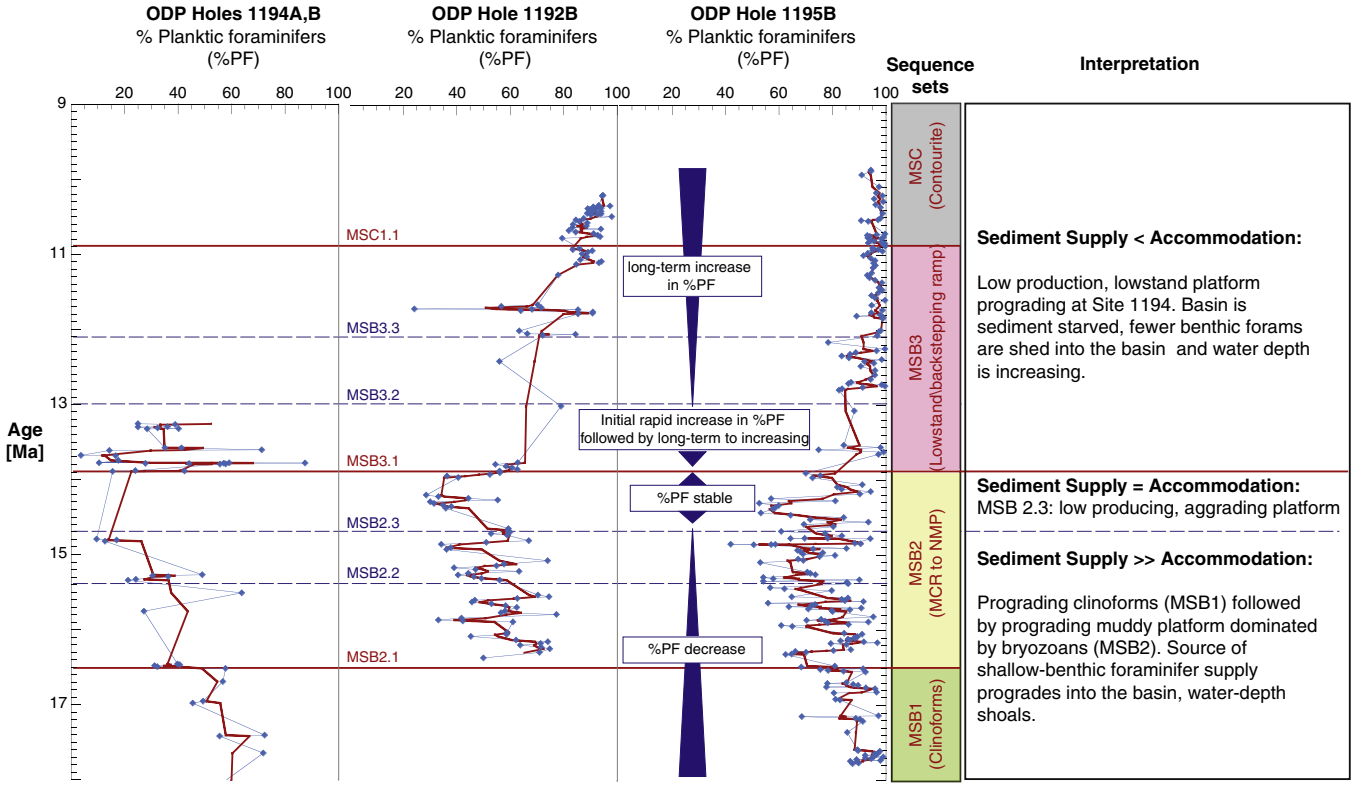

Fig. 5. % planktic foraminifers (percent of planktic foraminifers relative to the total foraminifer population) plotted against age at ODP sites 1194, 1192, and 1195. The red line is a 3 points running average of the data. Geologic interpretation of each zone is provided on the right of the figure. The continuous horizontal red lines trace the sequence sets boundaries, and dashed blue lines trace individual sequence boundaries.

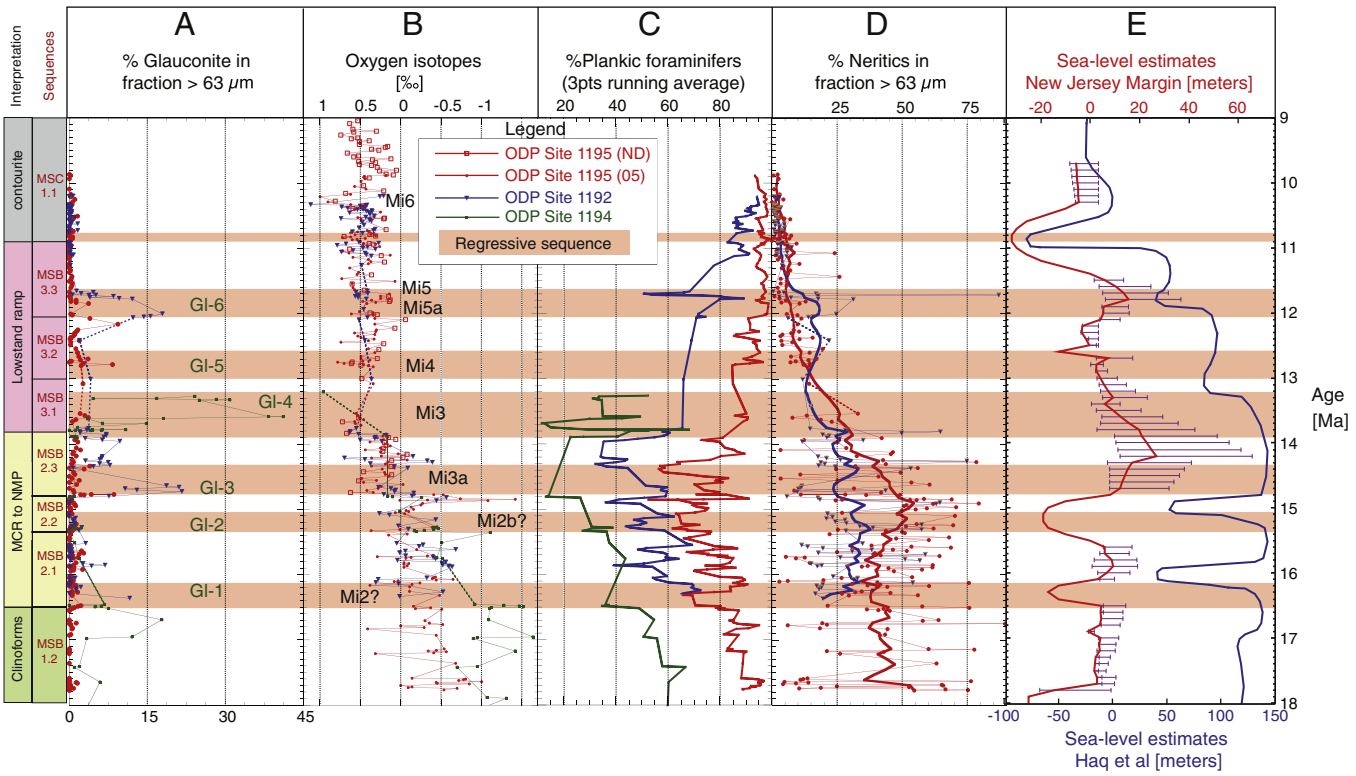

Fig. 6. Temporal evolution of A: Oxygen isotope (data from (John and Mutti, 2005), full circle, and this study, open squares); B: % glauconite (this study); C: 3 points running average of the % Planktic foraminifers data; D: Temporal evolution of % neritic fragments in the size fraction >63 μm at sites 1195 and 1192; E: Sea-level estimates from the Haq et al. (1987, 1988), curve (blue curve) and New Jersey Margin (red curve, Kominz et al., 2008). For panels A to D, data in green are from ODP hole 1194A and 1194B, in blue from ODP Hole 1192B, and in red from ODP Hole 1195B. Glauconite layers discussed in this paper are named in panel A, and isotopic events are indicated in panel B. The base of the orange bars corresponds to the sequence boundaries identified on the Marion Plateau, both in core and on seismic lines.

developed for tropical carbonate systems dominated by corals. This model predicts that maximum carbonate production will occur during highstands when the platform top is flooded and minimum during lowstands when the platform top is exposed and the carbonate factory is significantly reduced. The highstand shedding theory is supported on the Marion Plateau by the fact that sequence boundaries 2.3 and 3.1 are associated with sharp decreases in % neritic (Fig. 6D). We interpret this as a signal that the NMP platform was exposed and carbonate productivity greatly reduced during lowstands. However, it was also proposed that sediment condensation and accumulation of verdine, a green clay mineral similar to glauconite, in Plio-Pleistocene sequences from the mixed carbonate-siliciclastic Queensland margins occurred during major transgressions (Kronen and Glenn, 2000). In our study, the tie between core and seismic data demonstrates that glauconite layers associated with sequence boundaries on the Marion Plateau (Fig. 6) represent surfaces of correlative conformity on the periplatform (Catuneanu, 2006), that is, correlative to the subaerial exposures at the platform top. We note that not all of the glauconite layers occur at the base of a sequence (Fig. 6), and we assume that these layers represent either reworking of lowstand glauconite during the subsequent transgression or condensation of distal slope sequences during a rapid transgression and highstands, or a combination of both.

The % PF has long been suggested as a proxy for water depth: the greater the distance from shore (and thus the greater the water-depth), the greater the flux of planktic foraminifers and therefore the higher the % PF (Grimsdale and Van Morkhoven, 1955). The % PF has been successfully used as a qualitative proxy for paleo water-depth in different continental margin settings (Gibson, 1989, Kafescoglu, 1975, Leckie and Olson, 2003, Murray, 1976, Poag, 1972, Uchio, 1960, Van Marle et al., 1987), However, changes in % PF along a continental margin are not simply a function of water-depth per se; lateral shifts of coastal water masses, water mass fronts, foci of seasonal productivity, flux of organic matter to the seafloor in response to changes in relative sea level, and proximity of a shallow neritic source of benthic foraminifers (such as a carbonate platform) can also affect the % PF (Leckie and Olson, 2003). In effect, highstands (when shedding of the platform is at its maximum) may result in decreased percentage of planktics relative to benthics, thereby looking like lowered sea level, while lowstands may show increased % PF and resemble higher sea level on account of fewer neritic benthic foraminifers being shed off the carbonate platform.

The long-term changes in % PF (Figs. 5 and 6D) is consistent with observations from seismic data: sequences MSB1.1, MSB1.2 and MSB2.2 show evidence of progradation, and are associated with a decrease in % PF (i.e., shoaling upward sequence and/or increased shedding of neritic benthic foraminifers due to the progradation of the platform). Conversely, sequence MSB2.3, the aggrading NMP platform, shows a major increase in % PF coupled with a decrease in % neritic at the sequence boundary (exposure of the platform; decrease in the flux of benthic foraminifers) followed by relatively low and stable % PF (aggradation). Sequence set MSB3, characterized by aggradation and retrogradation of the lowstand ramp following a major eustatic drop, shows a sharp increase in the % PF coupled with a decrease in % neritic (Fig. 6C and D), and a long-term increase in % PF suggesting downing of the ramp as evidenced in cores and seismic data. The short-term trend in the % PF (Fig. 6C) is more ambiguous, but suggests that most sequence boundaries (i.e. MSB2.3 and MSB3.1) are associated with an initial increase in % PF (exposure of the platform) followed by a gradual decrease (recovery of the carbonate system during the transgression and following highstand).

5.2. Demonstrating eustatic forcing of Marion Plateau sequences

The sequence boundaries identified on seismic data and recognized in the cores by sediment condensation correspond to global Miocene oxygen isotope events (Mi-events = $\delta^{18}O$ maxima) as defined by Miller et al. (1991a,b, Fig. 6B). This is significant because the principal mechanism for eustatic variations during the Neogene is the waxing and waning of large high-latitude ice sheets (a mechanism known as "glacio-eustasy") (Miller et al., 2005). The correspondence between heavier $\delta^{18}O$ values, indicating more ice and colder climate, and sequence boundaries is a direct evidence of a eustatic control for the sequences from the Marion Plateau. The boundaries (i.e., bases) of sequences MSB2.1, MSB2.2, MSB2.3 and MSB3.1 correspond respectively to $\delta^{18}O$ events Mi2a, Mi2b, Mi3a, and Mi3. Hence, we demonstrate eustatic forcing of Marion Plateau sequences by establishing a direct link between sequence stratigraphic surfaces and growth phases of the East Antarctic ice sheet ($\delta^{18}O$ maxima) during the Miocene.

Furthermore, we recognize within sequence set MSB3 two smaller increases in $\delta^{18}O$ that we assign to events Mi4 (13.0 Ma) and a precursor to Mi5 (Mi5a, 12.1 Ma, Fig. 6B). Both of these $\delta^{18}O$ events are associated with a glauconite layers (Gl 5 and Gl 6) and with increases in % PF. The $\delta^{18}O$ events can also be seen in orbitally-tuned $\delta^{18}O$ records (Westerhold et al., 2005), although our ages differ slightly. No truncation of reflectors can be seen in the seismic data, but we argue that this is largely due to the low resolution of the seismic data within the condensed MSB3 sequence set. Thus, due to the similarity between the sedimentary response of events Mi4 and Mi5 and other seismic-scale sequence boundary, we associate events Mi4 and Mi5 with sequence boundaries MSB3.2 and MSB3.3 (Fig. 6B). The final demise of the Lowstand ramp corresponds to the base of Megasequence C at 10.9 Ma. Event Mi6 (Turco et al., 2001, Westerhold et al., 2005, Wright and Miller, 1992) is observed within Megasequence C at sites 1192 and 1195 (Fig. 6B), but it is not associated with a sequence boundary. The lack of response of the sedimentary system at 10.9 Ma is probably due to the nature of the sediment characterized by contourite deposits instead of carbonate platform and associated periplatform deposits.

The timing between sequences on the various published sea-level curves and the Marion Plateau is remarkably similar (Table 2), reinforcing a global mechanism for sequence formations at these locations. From 18.0 to 10.9 Ma, the Marion Plateau records all of the sequences identified on the New Jersey margin curve (Miller et al., 2005) as well as the sequences from the Queensland Plateau (Betzler et al., 2000), Great Bahamas Bank (Eberli et al., 2002), Gulf of Papua (Tcherepanov et al., 2008), and the Haq et al. (1987, 1988) curve (Table 2). Although it has been recognized that the Marion Plateau stratigraphic record is influenced by eustasy as well as the direction and strength of oceanic currents (Isern et al., 2004, John and Mutti, 2005), previous work also pointed out that Megasequence B did not show evidence of truncation by oceanic currents (Isern et al., 2004). The timing of the sequences on the Marion Plateau provides additional support for the argument that they are mainly controlled by eustasy. It is possible that oceanic currents started to be prevalent on the Marion Plateau within sequence MSB3.2 (John and Mutti, 2005), which would be consistent with the observation of current-controlled mound shape geometries similar to those described in the Maldives (Betzler et al., 2009). However, sequence set MSB2 and sequence MSB3.1 do not show evidence of current scour and therefore represent eustasy.

5.3. Amplitude estimates for Miocene eustasy

The recognition of surfaces that have a platform to slope geometry suitable for backstripping (i.e., sequence boundaries MSB2.1, MSB2.2, MSB2.3 and MSB3.1) in addition to the paleowater depth estimates for the period 18.0–13.9 Ma (Hallock et al., 2006, Isern et al., 2002) allows us to flexurally backstrip the surfaces to estimate the magnitude of sea-level fall as a function of time.

The backstripping analysis consists of the following steps (Table S3). First, for each interface, we flexurally remove the entire sediment column above the surface in question. Bulk sediment densities are calculated using the observed laboratory and logging density estimates for each site (Isern et al., 2002) using a least-squares curve fit to these data. Because the flexural strength of extended continental crust is controversial, we used a 10–40 km range in flexural strength, Te (e.g., Watts, 2001). We then used the fourth-order elastic differential equation (e.g., Karner et al., 1993) to estimate the flexural rebound across sites 1193, 1194, 1192 and 1195 induced by the various sediment and water loads:

a) Sediment loads:

$$D\frac{d^4w(x)}{dx^4} + (\rho_m - \rho_w)gw(x) = [\rho_s(x) - \rho_w]gs(x) \quad (1)$$

b) Water loads:

$$D\frac{d^4w(x)}{dx^4} + \rho_m gw(x) = \rho_w gb(x) \quad (2)$$

where D is the flexural rigidity of the lithosphere (considered spatial constant in this application), g is the acceleration of gravity, $\rangle_m$, $\rangle_s(x)$, and $\rangle_w$ are the mantle, sediment and water densities, respectively, s (x) and b(x) are the geometries of the sediment and water loads, respectively, and w(x) is the flexural uplift engendered by removing either the late early Miocene sediment or water loads from across the Marion Plateau. Flexural rigidity is related to Te by:

$$D = ETe^3 / 12(1-\nu^2) \quad (3)$$

where E is Young's modulus and ν is Poisson's ratio. With the removal of the sediment load across the plateau, we have a water-filled region of several 100 m's water. However, the removal of the overlying sediment will induce decompaction expansion of the underlying sediments. Sediment decompaction will reduce to some degree this accommodation. Using the sediment compaction estimates and trends measured from both laboratory and logging measurements from each drilling site (Isern et al., 2002), a regression curve was fitted to the sediment porosity data from each site and used to correct the water depth variation across the margin due to sediment decompaction.

From this reconstructed variation of water depth across the margin, we now reduce the sea-level to conform with the paleowater depth estimates at site 1193, the shallowest of the four sites analyzed and therefore with the minimum range in paleowater depth estimates based on benthic foraminifers (Hallock et al., 2006, Isern et al., 2002). This represents the paleowater depth during the highstand at site 1193. Because this change in water depth represents a constant sea-level change across the region, the calculation assumes local isostasy. We then reduce the sea-level flexurally to match the paleo-water depth estimates at sites 1193 and 1194 and the general paleo-water depths at sites 1192 and 1195.

With this scheme, we estimate eustatic falls of 47.7–73.7 m, 23.6–31.2 m, 20.7–21.6 m, and 20.8–21.1 m for the MSB3.1 (13.9 Ma), MSB2.3 (14.7 Ma), MSB2.2 (15.4 Ma) and MSB2.1 (16.5 Ma) events, respectively. A further correction needs to be made to the sea-level fall estimates summarized in step 5), and is associated with the regional thermal subsidence of the Marion Plateau during the time intervals of the sea level variations. Fig. S1 shows the backstripped subsidence and theoretical extension factors (δ upper plate; β lower plate thinning factors) for sites 1193, 1194, 1192 and 1195. It would seem that

1.6<β<1.8 captures the uplift and subsidence history for this region of the Marion Plateau, which implies a regional tectonic subsidence of 16–20 m over during 13–16 Ma. That is, a thermal subsidence component of 5–7 m/myr. These values need to be added to the eustatic fall estimates above. The corrected sea level variations for the four time intervals including the effects of thermal subsidence are (Fig. 7): 52.7–80.7 m (MSB3.1, 13.9 Ma), 28.6–38.2 m (MSB2.3, 14.7 Ma), 25.7–28.6 m (MSB2.2, 15.4 Ma), and 25.8–28.1 m (MSB2.1, 16.5 Ma). A similar approach as outlined above can be used to estimate the magnitude of eustatic rises in between the falls: 36.4–55.7 m (14.7–13.9 Ma), 19.8–28.6 m (15.4–14.7 Ma), and 17.8–19.8 m (16.5–15.4 Ma).

The backstripping estimates for the 13.9 Ma, 14.7 Ma and 15.4 Ma events are robust. However, we initially encountered a problem when quantifying the 16.5 Ma event. Honoring the shipboard paleowater depth at sites 1193 and 1194 (>100 m, Isern et al., 2002) resulted in a eustatic variation >70 m, which is unreasonable in view of the stable isotope constraints (see below). Reasonable backstripping estimates could be obtained when assuming 30 m of paleo-water depth at site 1193 prior to the fall. Estimating paleo-water depths within MSB1 is difficult because of the long-distance transport and abrasion of foraminifer, and possible reworking upslope of sediment (Isern et al., 2002). Thus, we suspect that the paleowater depth for this interval are questionable, and suggest that our backstripping solution for the 16.5 Ma fall is reasonable and compatible with stable isotope constraints. We acknowledge however that it is the least robust estimate from the Marion Plateau.

Oxygen isotopes can be used to check and further constrain the amplitude values obtained by backstripping. Oxygen isotopes will be influenced both by water temperature and ice volume (i.e., isotopic composition of seawater). Since both a cooling of the water and increased ice volume will drive the isotopic composition of calcite towards larger values, $\delta^{18}O_{\text{benthic foraminifers}}$ can be used as a maximum estimate of eustatic falls (see details in (John et al., 2004)). Using a thirteen point running average of the compilation data of oxygen isotopes for benthic foraminifer from Zachos et al. (2001), we estimate the successive change in $\delta^{18}O_{\text{benthic foraminifers}}$ to be 0.40‰ (16.5 Ma), 0.30‰ (15.4 Ma), 0.46‰ (14.7 Ma), and 0.65‰ (13.9 Ma). The sea-level rises are associated with decreases in $\delta^{18}O_{\text{benthic foraminifers}}$ of 0.3‰ (16.5–15.4 Ma), 0.27‰ (15.4–14.7 Ma), and 0.4‰ (14.7–13.9 Ma). Using the conversion rate between per mil value and meters of sea-level change established for the Pleistocene (0.1‰ for 10 m of sea-level change, Fairbanks and Matthews, 1978), we can estimate the 16.5–13.9 Ma events to represent up to 40 m, 30 m, 46 m and 65 m of sea-level fall, respectively (Fig. 7). Sea-level rises (from 16.5 to 13.9 Ma) are estimated at a maximum of 30 m, 27 m, and 40 m, respectively. The overlap between the backstripping and oxygen isotope estimates yields the best estimate for eustasy in the interval 16.5 Ma to 13.9 Ma (Fig. 7).

We construct two cumulative sea-level curves (Fig. 8): the first is a minimum sea-level curved based on the minimal range of backstripping estimates (Te = 10 km), the second is a reasonable maximum curve that combines backstripping and oxygen isotopes. Our data suggest that eustasy fell by 54–69 m during the 16.5–13.9 Ma

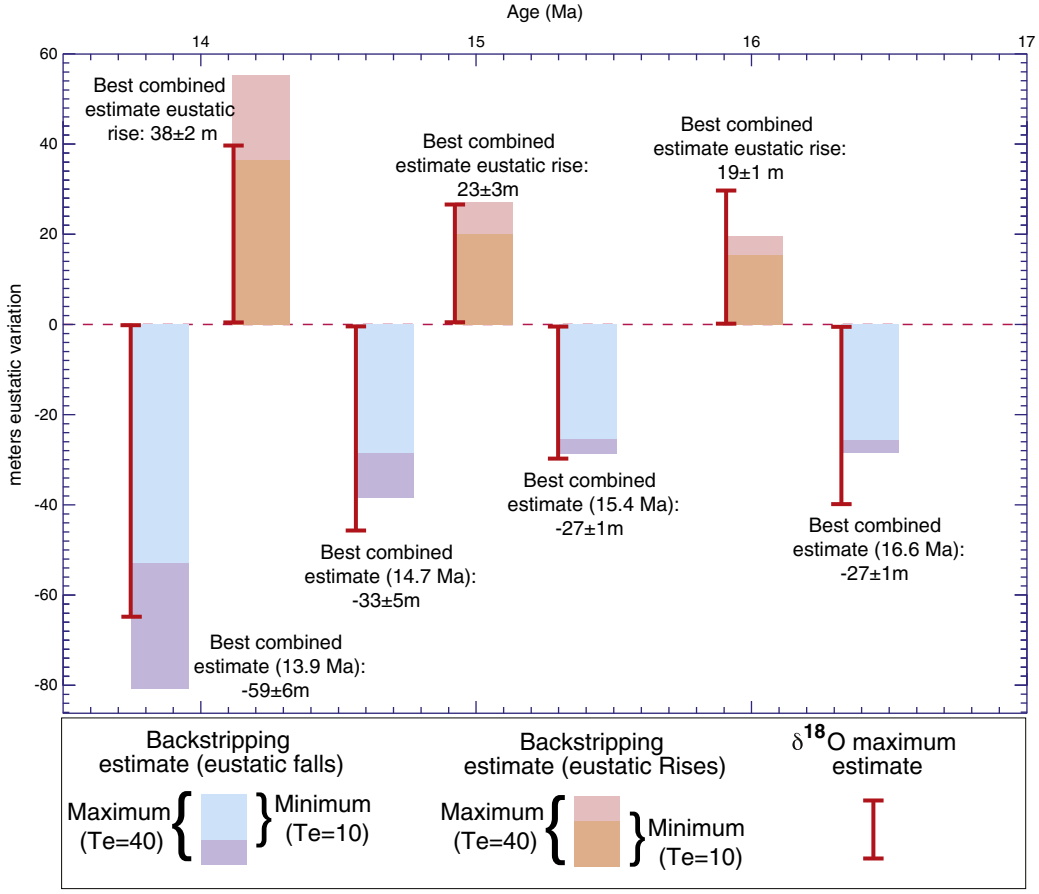

Fig. 7. Combined backstripping and oxygen isotopes amplitude estimates generated in our study. Minimum amplitude estimates from backstripping are based on the assumption of an effective flexural strength of the continental crust (Te) of 10 km, and maximum estimates assume a Te of 40 km. Oxygen isotope estimates are based on the amplitude of $\delta^{18}O$ variations on a global deep-sea compilation curve (Zachos et al., 2001). The best combined amplitude estimates are defined by the overlap between backstripping and oxygen isotopes constraints.

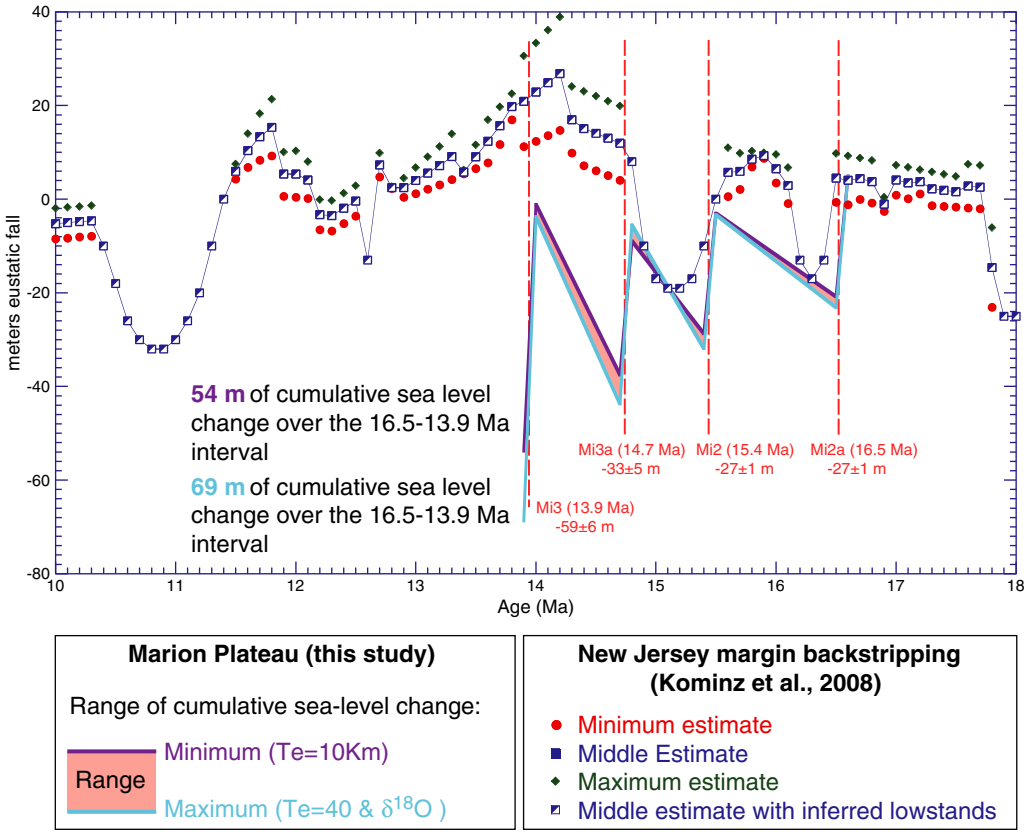

Fig. 8. Cumulative sea-level curve from the Marion Plateau compared with backstripping amplitude estimates from the New Jersey margin (Kominz et al., 2008). The minimal estimate curve from the Marion Plateau is obtained by adding the amplitudes of sea-level rises and falls obtained by backstripping with an effective flexural strength of the continental crust (Te) of 10 km. Maximum estimates from the Marion Plateau are obtained by adding the largest end-member of the best combined amplitude estimates (see Fig. 7).

interval. This implies that at least 89% of the East Antarctic ice sheet must have been established during the middle Miocene.

6. Conclusions

We recognize eight sequences on the Marion Plateau that are (within the resolution of our age model) correlative to sequences on the Queensland Plateau, New Jersey margin, Bahamas, and Gulf of Papua. This indicates that the sequence architecture preserved off the NMP is likely of eustatic origin. The Marion Plateau sequences are also correlative with deep-sea Miocene oxygen isotope events Mi2a, Mi2b, Mi3a, Mi3, Mi4, and Mi5 further linking the mixed carbonate-siliciclastic sequence architecture to episodes of ice volume increase during the Miocene.

The best geologic time window for estimating the amplitude of sea-level changes based on the NMP transect is from 16.5 to 13.9 Ma, when backstripping can be applied to a clinoform/platform-to-slope geometry. In sequence older than 16.5 Ma or younger than 13.9 Ma, backstripping cannot be applied due to the absence of carbonate platforms or clear clinoform geometries. Our estimates for the 16.5 Ma (MSB2.1) and 15.4 Ma (MSB2.2) events are comparable to the amplitude reported on the New Jersey margin, but our amplitude estimates for the 14.7 Ma (MSB2.3) and 13.9 Ma (MSB3.1) events are larger. Our long-term estimates of the magnitude of eustatic changes (53–69 m of sea-level fall between 16.5 and 13.9 Ma) are considerably more than what was predicted from the New Jersey margin (2–5 m eustatic rise, Fig. 8, Kominz et al. 2008). We argue that this results largely from the fact that estimates for the New Jersey margin rely on poorly recovered Miocene lowstand sequences, and are thus to be regarded as minimum estimates.

Supplementary materials related to this article can be found online at doi: 10.1016/j.epsl.2011.02.013.

Acknowledgements

Acknowledgement is made to the American Chemical Society - Petroleum Research Fund for major research support awarded to R.M. Leckie and C.M. John (PRF#48462-AC8). Ken Miller, Damian O'Grady (ExxonMobil), and an anonymous reviewer are thanked for their constructive reviews that help shape the manuscript. We thank Margaret Hastedt, Bill Crowford, Jonathan Strand and Amanda Ulincy for their help with scanning the cores from ODP Leg 194.

References

Abreu, V.S., Anderson, J.B., 1998. Glacial eustasy during the Cenozoic; sequence stratigraphic implications. AAPG Bulletin 82, 1385–1400.
Bartek, L.R., Vail, P.R., Anderson, J.B., Emmet, P.A., Wu, S., 1991. Efect of Cenozoic ice-sheet £uctuations in Antarctica on the stratigraphic signature of the Neogene. Journal of Geophysical Research 96, 6753–6778.
Betzler, C., Kroon, D., Reijmer, J.J.G., 2000. Synchroneity of major late Neogene sea level fluctuations and paleoceanographically controlled changes as recorded by two carbonate platforms. Paleoceanography 15, 722–730.
Betzler, C., Hübscher, C., Lindhorst, S., Reijmer, J.J.G., Römer, M., Droxler, A.W., Fürstenau, J., Lüdmann, T., 2009. Monsoonal-induced partial carbonate platform drowning (Maldives, Indian Ocean). Geology 37, 867–870.
Billups, K., Schrag, D.P., 2002. Paleotemperatures and ice volume of the past 27 Myr revisited with paired Mg/Ca and $^{18}O/^{16}O$ measurements on benthic foraminifera. Paleoceanography 17 (3–1), 3–11.
Browning, J.V., Miller, K.G., McLaughlin, P.P., Kominz, M.A., Sugarman, P.J., Monteverde, D., Feigenson, M.D., Hernández, J.C., 2006. Quantification of the effects of eustasy, subsidence, and sediment supply on Miocene sequences, mid-Atlantic margin of the United States. Geological Society of America Bulletin 118, 567–588.
Camoin, G.F., Iryu, Y., McInroy, D., Asami, R., Braaksma, H., Cabioch, G., Castillo-Paterno, R., Cohen, A.L., Cole, J.E., Deschamps, P., Fairbanks, R.G., Felis, T., Fujita, K., Hathorne, E.C., Lund, S.P., Machiyama, H., Matsuda, H., Quinn, T.M., Sugihara, K., Thomas, A.,

Vasconcelos, C.d.O., Verwer, K., Webster, J.M., Westphal, H., Woo, K.S., Yamada, T., Yokoyama, Y., 2007. Integrated Ocean Drilling Program Expedition 310 preliminary report; Tahiti sea level; the last deglacial sea level rise in the South Pacific; offshore drilling in Tahiti (French Polynesia); cruise dates, 6 October-16 November 2005; onshore science party, 13 February-4 March 2006, IODP Management international, College Station, TX.

Catuneanu, O., 2006. Principles of sequence stratigraphy. Elsevier, Amsterdam. 375 pp.

deKaenel, E., Villa, G., 1996. Oligocene-Miocene calcareous nannofossil biostratigraphy and paleoecology from the Iberia abyssal plaine. In: Whitmarsh, R.B., Sawyer, D.S., Klaus, A., Masson, D.G. (Eds.), Proceeding of the ODP, Scientific Results 149. Ocean Drilling Program, College Station, TX, pp. 79–145.

Eberli, G.P., Swart, P.K., Malone, M.J., et al., 1997. Proceeding of the ODP. Initial Report 166. Ocean Drilling Program, College Station, TX.

Eberli, G.P., Anselmetti, F.S., Kroon, D., Sato, T., Wright, J.D., 2002. The chronostratigraphic significance of seismic reflections along the Bahamas Transect. Marin Geology 185, 1–17.

Ehrenberg, S.N., McArthur, J.M., Thirlwall, M.F., 2006. Growth, demise, and dolomitization of Miocene carbonate platforms on the Marion Plateau, offshore NE Australia. Journal of Sedimentary Research 76, 91–116.

Fairbanks, R.G., Matthews, R.K., 1978. The Marine Oxygen Isotope Record in Pleistocene Coral, Barbados, West Indies. Quaternary Research 10, 181–196.

Fulthorpe, C.S., Miller, K.G., Droxler, A., Hesselbo, S.P., Camoin, G.F., Kominz, M.A., 2008. Drilling to Decipher Long-Term Sea-Level Changes and Effects—A Joint Consortium for Ocean Leadership, ICDP, IODP, DOSECC, and Chevron Workshop Scientific Drilling, pp. 19–28.

Gibson, T.G., 1989. Planktonic benthonic foraminiferal ratios: modern paterns and Tertiary applicability. Marine Micropaleontology 15, 29–52.

Gradstein, F.M., Ogg, J.G., Smith, A.G., et al., 2005. A Geologic Time Scale 2004. Cambridge University Press. 610 pp.

Grimsdale, T.F., Van Morkhoven, F.P.C.M., 1955. The Study of material from recent environments as a means of estimating depth of deposition of sedimentary rocks. 4th World Petrographic Congress Section I/D4, Rome, pp. 473–491.

Hallock, P., Sheps, K., Chaproniere, G., Howell, M., 2006. Larger benthic foraminifers of the Marion Plateau, northeastern Australia (ODP Leg 194): comparison of faunas from bryozoan (Sites 1193 and 1194) and red algal (Sites 1196–1198) dominated carbonate platforms. In: Anselmetti, F.S., Isern, A.R., Blum, P., Betzler, C. (Eds.), Proceeding of ODP, Scientific Results 194, Ocean Drilling Program, College Station, TX, pp. 1–31.

Haq, B.U., Hardenbol, J., Vail, P.R., 1987. Chronology of fluctuating sea levels since the Triassic. Science 235, 1156–1167.

Haq, B., Hardenbol, J., Vail, P., 1988. Mesozoic and Cenozoic chronostratigraphy and cycles of sea-level change. In: Wilgus, C., Hastings, B., Ross, C., Posamentier, H., Van Wagoner, J., Kendall, C. (Eds.), Sea-level changes; an integrated approach, Special Publication - Society of Economic Paleontologists and Mineralogists. 42, SEPM (Society for Sedimentary Geology), Tulsa, OK United States, pp. 72–108.

Holbourn, A., Kuhnt, W., Schulz, M., Flores, J.-A., Andersen, N., 2007. Orbitally-paced climate evolution during the middle Miocene "Monterey" carbon-isotope excursion. Earth and Planetary Science Letters 261, 534–550.

Isern, A.R., Anselmetti, F.S., Blum, P., Andresen, N., Birke, T.K., Bracco Gartner, G.L., Burns, S.J., Conesa, G.A.R., Delius, H., Dugan, B., Eberli, G.P., Ehrenberg, S., Fuller, M.D., Muller, P.H., Hine, A.C., Howell, M.W., John, C.M., Karner, G.D., Kindler, P.F., Olson, B.E., Sasaki, K., Stewart, D., Wei, W., White, T.S., Wood, J.L., Yamada, T., 2002. Proceedings of the Ocean Drilling Program, Initial Reports, 194 [CD-ROM]. Available from: Ocean Drilling Program, Texas A&M University, College Station TX 77845-9547, USA.

Isern, A.R., Anselmetti, F.S., Blum, P., 2004. A Neogene carbonate platform, slope, and shelf edifice shapred by sea levela nd ocean currents, Marion Plateau (Northeast Australia), Seismic imaging of carbonate reservoirs and systems. AAPG Memoir 81, 291–307.

John, C.M., Mutti, M., 2005. The response of heterozoan carbonate systems to Paleoceanographic, climatic and eustatic changes: a perspective from slope sediments of the Marion Plateau (ODP Leg 194). Journal of Sedimentary Research 75, 51–65.

John, C.M., Karner, G.D., Mutti, M., 2004. $\delta^{18}O$ and Marion Plateau backstripping: combining two approaches to constrain late middle Miocene eustatic amplitude. Geology 32, 829–832.

Kafescoglu, I.A., 1975. Quantitative distribution of foraminifera on the continental shelf and uppermost slope off Massachussetts. Micropaleontology 21, 261–305.

Karner, G.D., Driscoll, N.W., Weissel, J.K., 1993. Response of the lithosphere to in-plane force variations. Earth and Planetary Science Letters 114, 397–416.

Kominz, M.A., Browning, J.V., Miller, K.G., Sugarman, P.J., Mizintsevaw, S., Scotese, C.R., 2008. Late Cretaceous to Miocene sea-level estimates from the New Jersey and Delaware coastal plain coreholes: an error analysis. Basin Research.

Kronen, J.D., Glenn, C.R., 2000. Pristine to reworked minerals of the verdine facies: Keys to interpretating sequence stratigraphy and sequence condensation in mixed carbonate-siliciclastic forereef sediments (Great Barrier Reef). In: Glenn, C.R., Prévôt-Lucas, L., Lucas, J. (Eds.), Marine Authigenesis: From Global to Microbial Special Publication No. 66. Society for Sedimentary Geology, Tulsa, Ok, pp. 387–403.

Leckie, R.M., Olson, H., 2003. Foraminifera as proxies of sea-level change on siliciclastic margins. In: Olson, H.C., Leckie, R.M. (Eds.), Micropaleontologic Proxies of Sea-Level Change and Stratigraphic Discontinuities, Special Publication, SEPM (Society of Sedimentary Geology), Tulsa, pp. 5–19.

McArthur, J.M., Howarth, R.J., 2004. Sr-isotope stratigraphy. In: Gradstein, F., Ogg, J., Smith, A.G. (Eds.), A Geological Timescale 2004. Cambridge University Press, Cambridge, U.K., pp. 96–105.

Miller, K.G., Fairbanks, R.G., Mountains, G.S., 1987. Tertiary oxygen isotope synthesis, sea level history, and continental margin erosion. Paleoceanography 2, 1–19.

Miller, K.G., Feigenson, M.D., Wright, J.D., Clement, B.M., 1991a. Miocene isotope reference section, Deep Sea Drilling Project Site 608; an evaluation of isotope and biostratigraphic resolution. Paleoceanography 6, 33–52.

Miller, K.G., Wright, J.D., Fairbanks, R.G., 1991b. Unlocking the ice house: Oligocene-Miocene oxygen isotopes, eustasy, and margin erosion. Journal of Geophysical Research 69, 6829–6848.

Miller, K.G., Mountain, G.S., Browning, J.V., Kominz, M., Sugarman, P.J., Christie-Blick, N., Katz, M.E., Wright, J.D., 1998. Cenozoic global sea level, sequences, and the New Jersey transect; results from coastal plain and continental slope drilling. Reviews of Geophysics 36, 569–601.

Miller, K.G., Kominz, M.A., Browning, J.V., Wright, J.D., Mountain, G.S., Katz, M.E., Sugarman, P.J., Cramer, B.S., Christie-Blick, N., Pekar, S.F., 2005. The Phanerozoic record of global sea-level change. Science 312, 1293–1298.

Mountain, G.S., Miller, K.G., Blum, P., Aim, P.-G., Aubry, M.-P., Burckle, L.H., Christensen, B.A., Compton, J., Damuth, J.E., Deconinck, J.-F., Verteuil, L.d., Fulthorpe, C.S., Gartner, S., Guèrin, G., Hesselbo, S.P., Hoppie, B., Katz, M.E., Kotake, N., Lorenzo, J.M., McCracken, S., McHugh, C.M., Quayle, W.C., Saito, Y., Snyder, S.W., Kate, W.G.t., Urbat, M., Van Fossen, M.C., Vecsei, A. (Eds.), 1994. Initial reports, New Jersey Continental Slope and Rise. Ocean Drilling Program.

Mountain, G.S., Proust, J.-N., McInroy, D., 2009. New Jersey shallow shelf: shallow-water drilling of the New Jersey continental shelf: global sea level and achitecture of passive margin sediments. IODP-MI, College Station, TX.

Murray, J.W., 1976. A method of determining proximity of marginal seas to an open ocean. Marine Geology 22, 103–119.

Mutti, M., John, C.M., Knoerich, A.C., 2006. Chemistratigraphy in Miocene heterozoan carbonate settings; applications, limitations and perspectives. In: Pedley, H.M., Carannante, G. (Eds.), Cool-water carbonates; depositional systems and palaeoenvironmental controls. Geological Society of London, London, pp. 307–322.

Nathan, S.A., Leckie, R.M., 2009. Early history of the Western Pacific Warm Pool during the middle to late Miocene (approximately 13.2-5.8 Ma); role of sea-level change and implications for equatorial circulation. Palaeogeography, Palaeoclimatology, Palaeoecology 274, 140–159.

Oslick, J.S., Miller, K.G., Feigenson, M.D., Wright, J.D., 1994. Oligocene-Miocene strontium isotopes; stratigraphic revisions and correlations to an inferred glacioeustatic record. Paleoceanography 9, 427–443.

Pitman, W.C., Golovchenko, X., 1983. The effect of sealevel change on the shelfedge and slope of passive margins. In: Stanley, D.J., Moore, G.T. (Eds.), The shelfbreak; critical interface on continental margins 33. Special Publication, 33. Society of Economic Paleontologists and Mineralogists, pp. 41–58.

Poag, C.W., 1972. Shelf-edge submarine banks in teh Gulf of Mexico: paleoecology and biostratigraphy. Gulf Coast Ass. Pet. Geol. Bull. 48, 1810–1827.

Posamentier, H.W., Jervey, M.T., Vail, P.R., 1988. Eustatic controls on clastic deposition; I, Conceptual framework. In: Wilgus, C.K., Hastings, B.S., Ross, C.A., Posamentier, H.W., Van Wagoner, J., Kendall, C.G.S.C. (Eds.), Sea-level changes; an integrated approach. Special Publication, 42. Society of Economic Paleontologists and Mineralogists, pp. 109–124.

Raffi, I., Backman, J., Fornaciari, E., Pälike, E., Rio, D., Lourens, L., Hilgen, F., 2006. A review of calcareous nannofossil astrobiochronology encompassing the past 25 million years. Quaternary Science Reviews 3113–3137.

Schlager, W., Reijmer, J.J.G., Droxler, A., 1994. Highstand shedding of carbonate platforms. Journal of Sedimentary Research 64, 27–281.

Shevenell, A.E., Kennett, J.P., Lea, D.W., 2004. Middle Miocene Southern Ocean Cooling and Antarctic Cryosphere Expansion. Science 305, 1766–1770.

Shevenell, A.E., Kennett, J.P., Lea, D.W., 2008. Middle Miocene ice sheet dynamics, deep-sea temperatures, and carbon cycling: A Southern Ocean perspective. Geochemistry, Geophysics, Geosystems - G3 (9), Q02006.

Tcherepanov, E.N., Droxler, A.W., Lapointe, P., Mohn, K., 2008. Carbonate seismic stratigraphy of the Gulf of Papua mixed depositional system: Neogene stratigraphic signature and eustatic control. Basin Research 20, 185–209.

Turco, E., Hilgen, F.J., Lourens, L.J., Shackleton, N.J., Zachariasse, W.J., 2001. Punctuated evolution of global climate cooling during the late middle to early late Miocene: high-resolution planktonic foraminiferal and oxygen isotope records from the Mediterranean. Paleoceanography 16, 405–423.

Uchio, T., 1960. Ecology of living foraminifera from the San Diego, California, area. Cushmd Found. Foraminiferal Research Special Publications 5, 1–72.

Vail, P.R., Hardenbol, J., 1979. Sea-level change during the Tertiary. Oceanus 22, 71–79.

van Marle, L.J., Van Hinte, J.E., Nederbragt, A.J., 1987. Plankton percentage of the foraminiferal fauna in seafloor samples from the Australian-Irian Jaya continental margin, Eastern Indonesia. Marine Geology 77, 151–156.

Watkins, D.K., Bergen, J.A., 2003. Late Albian adaptive radiation in the calcareous nannofossil genus Effellithus. Micropaleontology 49, 231–252.

Watts, A.B., 2001. Isostasy and flexure of the lithosphere. Cambridge University Press. 478 pp.

Westerhold, T., Bickert, T., Roehl, U., 2005. Middle to late Miocene oxygen isotope stratigraphy of ODP Site 1085 (SE Atlantic); new constrains on Miocene climate variability and sea-level fluctuations. Palaeogeography, Palaeoclimatology, Palaeoecology 217, 205–222.

Wright, J.D., Miller, K.G., 1992. Miocene stable isotope stratigraphy, Site 747. Kerguelen Plateau.

Zachos, J., Pagani, M., Sloan, L., Thomas, E., Billups, K., 2001. Trends, rhythms, and aberrations in global climate 65 Ma to present. Science 292, 686–693.